Proceedings of the Twenty-eighth (2018) International Ocean and Polar Engineering Conference
Sapporo, Japan, June 10-15, 2018

ISBN 978-1-880653-87-6; ISSN 1098-6189

www.isope.org

Numerical Study of Solitary Wave Slamming on a 3-D Flexible Plate by MPS-FEM Coupled Method

*Guanyu Zhang, Chengping Rao, Decheng Wan**
Collaborative Innovation Center for Advanced Ship and Deep-Sea Exploration, State Key Laboratory of Ocean Engineering,
School of Naval Architecture, Ocean and Civil Engineering, Shanghai Jiao Tong University, Shanghai, China
*Corresponding author

ABSTRACT

In this paper, the simulation of the interaction between three-dimension solitary wave and horizontal plate is investigated using the moving particle semi-implicit and finite element coupled method (MPS-FEM). The MPS method is used to calculate the fluid domain, while the FEM is adopted to solve the structure domain. The simulation of solitary wave slamming onto the flexible plate is initially conducted, the effects of wave amplitude and plate elevation on the wave-induced impact force are investigated. The interaction between wave and flexible plate is finally compared with that regarding the rigid plate to study the contribution of the structural flexibility to the wave-induced force and energy dissipation.

KEY WORDS: Moving Particle Semi-Implicit; MPS-FEM coupled method; fluid–structure interaction (FSI); wave-induced force.

INTRODUCTION

Plate-like offshore structures, such as the pier, jetty and very large floating structure (VLFS), are vulnerable to fluid impact loads. Especially the VLFS, whose stiffness is relatively small, presents the similar behavior to that of a flexible plate above the water surface. When encountering extreme wave, the plate may produce elastic vibration and considerable deformation which would bring the new challenges for the structural safety. The study of Fluid-Structure interaction (FSI) problems due to the fluid impact loads onto the structures, becomes of paramount importance in the field of naval architecture and ocean engineering.

Experimental studies in FSI problems are scarce and there are only a few papers involved these problems, e.g. Cox et al. (2002), Guomo et al. (2007) and Nelli et al. (2017). In addition, various numerical methods have been conducted in order to simulate FSI problems. By using finite element method, Irahpanah (1983) simulated the impact of wave on horizontal platform, analyzed the wave-induced load at the bottom of the deck. Seiffert et al. (2014), based on finite volume method, simulated the solitary wave impacting on a horizontal plate with the help of an open source CFD software – OpenFOAM. The influence of the depth of the numerical flume, the plate elevation and the wave amplitude are investigated, the obtained results agreed well with the experiment data. However, there are much fewer FSI analysis about flexible plates. Liu et al. (2002) combined the boundary element method (BEM) and FEM to investigate the hydroelastic response of two-dimensional elastic plate under wave-induced force. Liao and Hu (2013) applied a coupled FDM–FEM method to investigate the interaction between surface flow and thin elastic plate, and obtained good results. Nelli (2017) conducted the experiment of the wave impacting a thin flexible plate, to analyze the reflection and transmission of regular incident water waves. It can draw a conclusion that the amplitude was attenuated due to the green water and wave breaking, and the attenuation is small when the plate is more flexible. Liu et al. (2018) conducts the quasi-static and dynamic tensile tests and plate impact experiments, demonstrates that the strain rate effect varies with the plastic strain and provides a practical advice for ship collision assessments.

Despite the effectiveness, these mesh-based methods may suffer from the difficulties such as the adjustment and regeneration of mesh while coordinating the interface between fluid and solid domain. Therefore, some newly mesh-free particle methods have drawn a great deal of attention. In contrast with the mesh-based method, these mesh-free methods are inherently Lagrangian methods, by which a continuum is discretized into moving particles, so that the calculation of the numerical dissipation of the convection term is avoided. In addition, the meshfree particle methods avert the treatment of mesh or the capture of free surface. Thus, meshfree particle methods can deal with the large deformation and strong nonlinear phenomenon of free surfaces with relative ease, as well as the moving boundaries. SPH (Smoothed Particle Hydrodynamics) proposed by Lucy (1977), is a traditional meshfree method, which was first applied in astrophysics. Subsequently, SPH has been developed more actively, and has been applied to incompressible flow and FSI problems in Antoci et al. (2007). In addition, some scholars managed to combine SPH with other methods

to solve the FSI problems. The SPH–FEM coupling method has been first proposed by Attaway et al. (1994) to investigated structure-structure interaction, but it was used in FSI problems soon afterwards (Fourey et al. 2012; Yang et al. 2012; Long et al. 2016). The MPS (Moving Particle Semi-implicit) proposed by Koshizuka and Oka (1996), is another typical particle-based meshfree method. Compared with the SPH, the pressure of the particle is obtained by solving the Poisson's pressure equation (PPE) in the MPS method. Thus, the obtained pressure field through MPS method is relatively smoother. MPS was later applied into the field of ocean engineering (Gotoh and Khayyer. 2016). Some preliminary researches corresponding to FSI has been conducted on the basis of the MPS method. The FEM method is a general choose to combine, in order to address complicated FSI problem. Lee et al. (2007) successfully simulated the interaction between dam-break and sloshing flow through the coupled MPS-FEM method. Some other research performing the MPS-FEM model (Mitsume et al. 2014; Hwang et al. 2014; Hwang et al. 2016; Zhang et al. 2016a) also displayed fair agreement with available experimental results.

The objective of the present paper is to investigate the slamming on a 3-D flexible plate induced by solitary wave using the MPS-FEM coupled method. A number of cases should be conducted because of the uncertainty regarding their occurrence and scale. The outline of the present paper is shown as follows. The theories of MPS, FEM and coupling strategy are briefly introduced. Subsequently, the simulation of 3-D solitary wave slamming onto the flexible plate is conducted, the effects of wave amplitude and plate elevation on the wave-induced impact force are investigated. Finally, the interaction between wave and flexible plate is finally compared with the rigid plate to study the contribution of the structural flexibility to the wave-induced force and energy dissipation.

NUMERICAL METHOD

In this study, the MPS-FEM coupled method is adopted to investigate the wave-plate interaction problem. The MPS method is used to calculate the fluid domain, while the FEM is adopted to solve the structure domain. Specifically, the 4-node thin plate element is employed in the FEM calculation, and a partitioned coupling strategy is adopted to unite the two methods. The theory for the MPS and FEM have been presented with details in our previous papers (Zhang and Wan, 2012; Zhang et al., 2014; Tang et al., 2015; Tang et al., 2016; Zhang et al., 2016b; Zhang and Wan. 2017; Zhang and Wan. 2018). These are introduced briefly in this section.

MPS formulation for fluid dynamics

The governing equations of the MPS method for viscous incompressible fluid can be expressed in Lagrangian form as following:

$$\nabla \cdot \boldsymbol{V} = 0 \tag{1}$$

$$\frac{\mathrm{D}\boldsymbol{V}}{\mathrm{D}t} = -\frac{1}{\rho}\nabla P + \nu \nabla^2 \boldsymbol{V} + \boldsymbol{g} \tag{2}$$

where $\boldsymbol{V}$, ρ, P, ν and $\boldsymbol{g}$ denote the velocity vector, the fluid density, the pressure, the kinematic viscosity and the gravitational acceleration. The kernel function in present paper can be formulated as:

$$W(r) = \begin{cases} \dfrac{r_e}{0.85r + 0.15r_e} - 1 & 0 \le r < r_e \\ 0 & r_e \le r \end{cases} \tag{3}$$

where $r = |\boldsymbol{r}_j - \boldsymbol{r}_i|$ is the distance between particle i and j, and r_e denotes the influence radius of the target particle. In MPS, the models of particle interaction involve the gradient, divergence, and Laplacian models. They are written as Eq. (4), Eq. (5) and Eq. (6).

$$\langle \nabla \phi \rangle_i = \frac{D}{n^0} \sum_{j \ne i} \frac{\phi_j + \phi_i}{|\boldsymbol{r}_j - \boldsymbol{r}_i|^2} (\boldsymbol{r}_j - \boldsymbol{r}_i) \cdot W(|\boldsymbol{r}_j - \boldsymbol{r}_i|) \tag{4}$$

$$\langle \nabla \cdot \boldsymbol{V} \rangle_i = \frac{D}{n^0} \sum_{j \ne i} \frac{(\boldsymbol{V}_j - \boldsymbol{V}_i) \cdot (\boldsymbol{r}_j - \boldsymbol{r}_i)}{|\boldsymbol{r}_j - \boldsymbol{r}_i|^2} W(|\boldsymbol{r}_j - \boldsymbol{r}_i|) \tag{5}$$

$$\langle \nabla^2 \phi \rangle_i = \frac{2D}{n^0 \lambda} \sum_{j \ne i} (\phi_j - \phi_i) \cdot W(|\boldsymbol{r}_j - \boldsymbol{r}_i|) \tag{6}$$

$$\lambda = \frac{\sum_{j \ne i} W\left(\left|\boldsymbol{r}_j - \boldsymbol{r}_i\right|\right) \left|\boldsymbol{r}_j - \boldsymbol{r}_i\right|^2}{\sum_{j \ne i} W\left(\left|\boldsymbol{r}_j - \boldsymbol{r}_i\right|\right)} \tag{7}$$

where D is the dimension number, $\boldsymbol{r}$ is the position vector, and n^0 is the initial density of the particle number and defined as:

$$\langle n \rangle_i = \sum_{j \ne i} W\left(\left|\boldsymbol{r}_j - \boldsymbol{r}_i\right|\right) \tag{8}$$

The pressure fields are obtained through solving the PPE. In present paper, the mixed source term method is employed combined with a velocity divergence-free condition and a constant particle number density (Tanaka et al., 2010 and Lee et al., 2011) as following:

$$\langle \nabla^2 P^{k+1} \rangle_i = (1-\gamma) \frac{\rho}{\Delta t} \nabla \cdot V_i^* - \gamma \frac{\rho}{\Delta t^2} \frac{< n^k >_i - n^0}{n^0} \tag{9}$$

where Δt denotes the calculation time step, k and $k+1$ indicate the physical quantity in the k th and $k+1$ th time steps, and γ is the weight of the particle number density term between 0 and 1. In this paper, γ =0.01 is selected for all numerical experiments.

FEM formulation for structure dynamics

Based on FEM theory, the spatially discretized structural dynamic equations, which govern the motion of structural nodes, can be formulated as:

$$\mathbf{M}\ddot{\boldsymbol{y}} + \mathbf{C}\dot{\boldsymbol{y}} + \mathbf{K}\boldsymbol{y} = \boldsymbol{F}(t) \tag{10}$$

$$\mathbf{C} = \alpha_1 \mathbf{M} + \alpha_2 \mathbf{K} \tag{11}$$

where $\boldsymbol{M}$, $\boldsymbol{C}$, $\boldsymbol{K}$ denote the mass matrix, the Rayleigh damping matrix, and the stiffness matrix of the structure, respectively. $\boldsymbol{F}$ is the external force vector that acts on the structure and varies with computational time. $\boldsymbol{y}$ is the displacement vector of the structure element node. α_1 and α_2 are coefficients related to the natural frequency and the damping ratios of the structure.

According to Newmark (1959), the structural node displacement at $t=t+\Delta t$ can be solved with the help of Taylor's expansions of velocity and displacement:

$$\dot{\boldsymbol{y}}_{t+\Delta t} = \dot{\boldsymbol{y}}_t + (1-\gamma)\ddot{\boldsymbol{y}}_t \Delta t + \gamma \ddot{\boldsymbol{y}}_{t+\Delta t} \Delta t,\ 0 < \gamma < 1 \tag{12}$$

$$\boldsymbol{y}_{t+\Delta t} = \boldsymbol{y}_t + \dot{\boldsymbol{y}}_t \Delta t + \frac{1-2\beta}{2} \ddot{\boldsymbol{y}}_t \Delta t^2 + \beta \ddot{\boldsymbol{y}}_{t+\Delta t} \Delta t^2, \quad 0 < \beta < 1 \tag{13}$$

where β and γ are paramount parameters in the Newmark-β method and are set as β=0.25, γ=0.5 for all simulations. Then the displacement at $t=t+\Delta t$ is proposed by Hsiao et al. (1999):

$$\bar{\mathbf{K}}\, \boldsymbol{y}_{t+\Delta t} = \bar{\boldsymbol{F}}_{t+\Delta t} \tag{14}$$

$$\bar{\mathbf{K}} = \mathbf{K} + a_0 \mathbf{M} + a_1 \mathbf{C} \tag{15}$$

$$\bar{\boldsymbol{F}}_{t+\Delta t} = \boldsymbol{F}_t + \mathbf{M}(a_0 \boldsymbol{y}_t + a_2 \dot{\boldsymbol{y}}_t + a_3 \ddot{\boldsymbol{y}}_t) + \mathbf{C}(a_1 \boldsymbol{y}_t + a_4 \dot{\boldsymbol{y}}_t + a_5 \ddot{\boldsymbol{y}}_t) \tag{16}$$

$$a_0=\frac{1}{\beta\Delta t^2},\ a_1=\frac{\gamma}{\beta\Delta t},\ a_2=\frac{1}{\beta\Delta t},\ a_3=\frac{1}{2\beta}-1,$$
$$a_4=\frac{\gamma}{\beta}-1,a_5=\frac{\Delta t}{2}(\frac{\gamma}{\beta}-2),\ a_6=\Delta t(1-\gamma),\ a_7=\gamma\Delta t \tag{17}$$

where $\bar{\mathbf{K}}$ and $\bar{F}$ denote the effective stiffness matrix and effective force vector. Subsequently, the accelerations and velocities related to the next time step are updated as follows:

$$\ddot{\boldsymbol{y}}_{t+\Delta t}=a_0(\boldsymbol{y}_{t+\Delta t}-\boldsymbol{y}_t)-a_2\dot{\boldsymbol{y}}_t-a_3\ddot{\boldsymbol{y}}_t \tag{18}$$

$$\dot{\boldsymbol{y}}_{t+\Delta t}=\dot{\boldsymbol{y}}_t+a_6\ddot{\boldsymbol{y}}_t+a_7\ddot{\boldsymbol{y}}_{t+\Delta t} \tag{19}$$

Coupling strategy for MPS-FEM coupled method

In this study, the weak coupling between MPS and the FEM method is implemented. The time step sizes for structure and fluid analyses are Δt_s and Δt_f, respectively. Due to the stability of Newmark-β scheme, Δt_s can be longer than Δt_f, so that Δt_s is k multiples of Δt_f, where k is an integer. The interaction procedure can be summarized as follows:

1) The pressure of the fluid wall boundary particle is calculated at each fluid time step. Then the pressure should be averaged during Δt_s, to obtain the external force on the element node, as follows:

$$\bar{p}_{n+1}=\frac{1}{k}\sum_{i=1}^{k}p_{n+i} \tag{20}$$

where p_{n+1} is the pressure of the fluid particle on the wall boundary at the instant $t+i\Delta t_f$, and $\bar{p}_{n+1}$ is the average pressure of the fluid particle within Δt_s.

2) The values of structural nodal position y_t, velocity $\dot{y}_t$, and acceleration $\ddot{y}_t$ can be determined based on the previous time step.

3) The external force vector $\boldsymbol{F}_{t+\Delta t_s}$ of the structural boundary particles is calculated by multiplying the average pressure $\bar{p}_{n+1}$ and the influential area, which equals the square of the initial particle spacing dp.

$$\boldsymbol{F}_{t+\Delta t_s}=\bar{p}_{n+1}\cdot dp^2 \tag{21}$$

4) The structural nodal displacements and velocities at next structural time step can be calculated based on the Newmark-β scheme.

5) Update the velocity and position of the structural boundary particles at each structural time step and the fluid particles at each fluid time step.

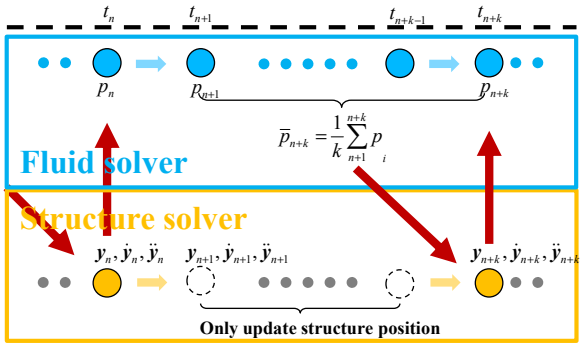

Fig. 1 Schematic diagram of the partitioned coupling strategy between the fluid and structure domains

Numerical wave generation

According to the potential flow theory, a solitary wave consists of a single crest of infinite length. The profile of the solitary wave can be expressed as follows (Korteweg and De Vries, 1895):

$$\eta=A\mathrm{sech}^2(k(x-ct)) \tag{22}$$

$$k=\sqrt{3A/4H^3} \tag{23}$$

$$c=\sqrt{g(A+H)} \tag{24}$$

where A is the water height, also is the wave amplitude for solitary wave. H, x and c denote the water depth, the horizontal coordinate and the wave speed, respectively. In this paper, the solitary wave is generated by a piston-type wavemaker, whose motion was described by Goring (1978). The speed of the wavemaker is formulated as:

$$U(t)=\frac{\mathrm{d}X(t)}{\mathrm{d}t}=\frac{cA\mathrm{sech}^2(k(X-ct))}{H+A\mathrm{sech}^2(k(X-ct))} \tag{25}$$

Thus, the position of the wavemaker at time t can be expressed as:

$$X(t)=\frac{A}{kH}\tanh(k(ct-X)) \tag{26}$$

The stroke length is calculated by the difference value between the wavemaker position at $t=+\infty$ and $t=-\infty$:

$$S=\sqrt{\frac{16AH}{3}} \tag{27}$$

The wave period is approximately:

$$T\approx\frac{2}{kc}(3.8+\frac{A}{H}) \tag{28}$$

After one wave period, the wavemaker reaches its maximum position and then becomes still.

NUMERICAL SIMULATION

In this section, the interaction of 3D solitary wave interacting with a flexible horizontal plate is investigated based on aforementioned MPS-FEM coupled method. Figure 2 shows the model of the numerical wave tank together with the plate. The tank is 2.00 m in length and the water depth (H) is 0.114m. As is shown, the left side of the tank is a piston-type wavemaker that is employed to generate the solitary wave. A fixed support horizontal plate is installed in the middle of the tank.

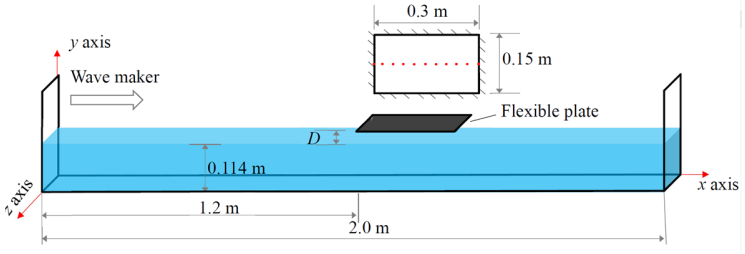

Fig. 2 Geometric model of the numerical wave tank

Numerical wave generations

Before studying the wave-structure interaction, it is of importance to examine the accuracy of the generated solitary wave, the verification is conducted in the numerical wave tank without the plate. The solitary wave, with different wave amplitudes (A), including A/H=0.2, 0.3, 0.4 and 0.5, adopted in the simulations. The computational parameters are listed in Table 1.

Table 1. The computational parameters of MPS

Parameter	Value
Water density	1000 kg/m^3

Kinematic viscosity	1×10^{-6} m^2/s
Gravitational acceleration	9.81 m/s^2
Particle spacing	0.0075 m
Fluid number	82614
Total number	156273

The surface elevation at wave amplitudes of A/H= 0.2~0.5 is depicted in Fig.3. The comparison of the wave profile between the numerical simulation and the theoretical solution shows that the wave crest of the simulation agrees well with those presented by Goring (1978).

Wave impacting onto flexible plate

In this subsection, the interaction between the three-dimension solitary wave and a flexible plate is simulated with the help of the in-house MPSFEM-SJTU solver. Two dimensional FSI problems has been simulated using MPSFEM-SJTU solver by Zhang et al. (2018) and Rao et al. (2017), and the obtained results are well reliable. The structural parameter is shown in Table 2. The elastic modulus of the plate is 50MPa. In addition, the distance between the bottom of the plate and the still water line (SWL) is defined as plate elevation (D), which can be altered by moving the plate vertically. In the simulations, the plate elevation (D) and wave amplitude (A) vary from case to case in order to investigate their effects on the wave-induced force on the plate. The dimensionless parameters of all the cases are shown in Table 3.

Figure 4 shows the particular snapshots of the interaction between solitary wave and flexible plate under the condition of A/H=0.3, D/H=0.1. The calculated wave-induced force on the plate is shown in Fig. 5 and the displacement history in the middle of the plate is shown in Fig.6. It can be seen that the plate possesses a slight upward deformation immediately as the wave contacts the plate around t=1.62s. Then the wave crest hits the leading edge of the plate at around 1.82s, and the vertical force reaches maximum. The maximum vertical force lasts about one second with slight oscillation, until 1.92s. Subsequently, the deformation reaches the maximum, and the force begins to descend without evident oscillation. Finally, the plate suffered a negative vertical force after t=2.08s owing to the green water on the plate. It can be easily observed that the horizontal force is far less than vertical force, which indicates that the interaction between wave and plate mainly reflects in vertical slamming.

Table 2. The computational parameters of FEM

Parameters	Values
Structural density	1800 kg/m^3
Elastic modulus	50 MPa
Thickness	0.001 m
Poisson's ratio	0.3
Damping coefficient α_1	0
Damping coefficient α_2	0
Element type	4-node thin plate element
Element number	800

Table 3. Configurations of the cases

Case No.	Amplitude (A/H)	Elevation (D/H)
1	0.2	0.06
2	0.2	0.12
3	0.3	0.06
4	0.3	0.12
5	0.3	0.18
6	0.4	0.06
7	0.4	0.12
8	0.4	0.18
9	0.5	0.06
10	0.5	0.12
11	0.5	0.18

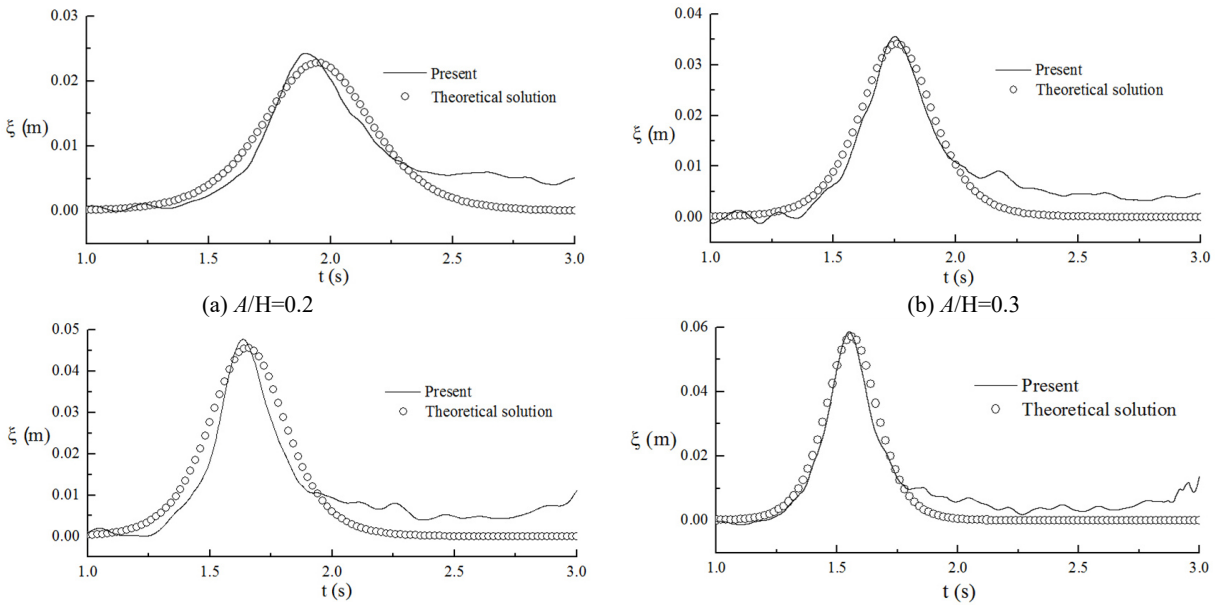

(a) A/H=0.2 (b) A/H=0.3

(c) A/H=0.4 (d) A/H=0.5

Fig. 3 The wave elevation on the wave gauge

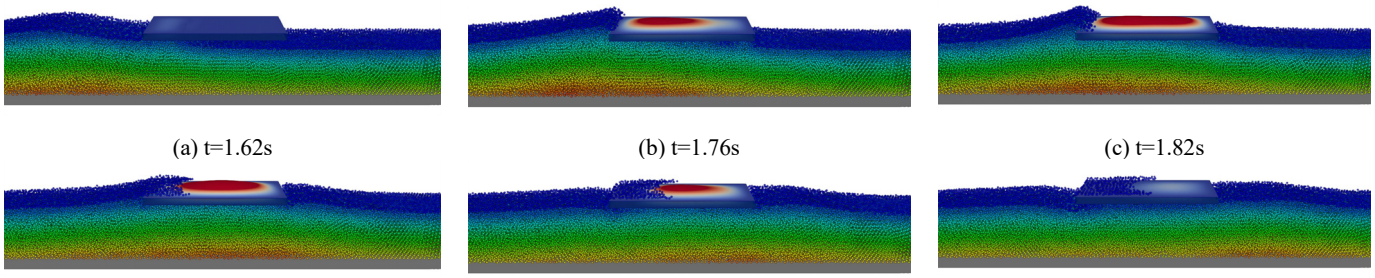

(a) t=1.62s (b) t=1.76s (c) t=1.82s

(d) t=1.92s (e) t=1.98s (f) t=2.04s

Fig. 4 Snapshots of wave-plate interaction (flexible plate)

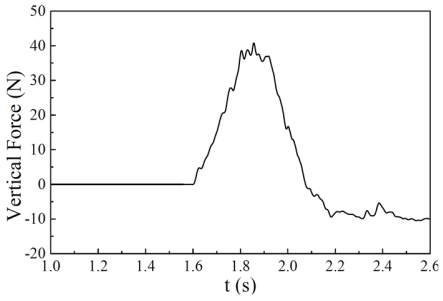

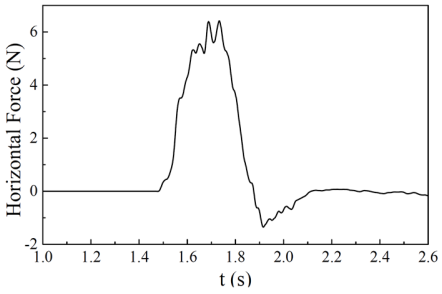

Fig. 5 wave-induced forces on the plate

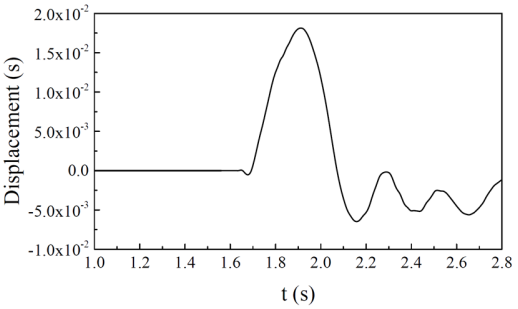

Fig. 6 displacement history on the middle of plate

To investigate the effects of the wave amplitude and plate elevation on the wave-induced force, especially the vertical slamming, the maximum value of vertical force history in each case is collected. It can be inferred in the Fig. 7 that the maximum vertical force on the plate is approximatively in proportion to the wave amplitude under the same plate elevations, while the maximum vertical force decreases with the plate elevation increasing. Similar to the results from Liu (2016), the force increases at first with the ascending of elevation, then goes down. The discrepancy in smaller elevation is owing to the finite depth of tank. In addition, the comparison of vertical force history under different plate elevations is depicted in Fig. 8, the loading duration increases with the ascending of the amplitude and the descending of the elevation. Besides, evident oscillation during the rise of force can be observed in a greater elevation.

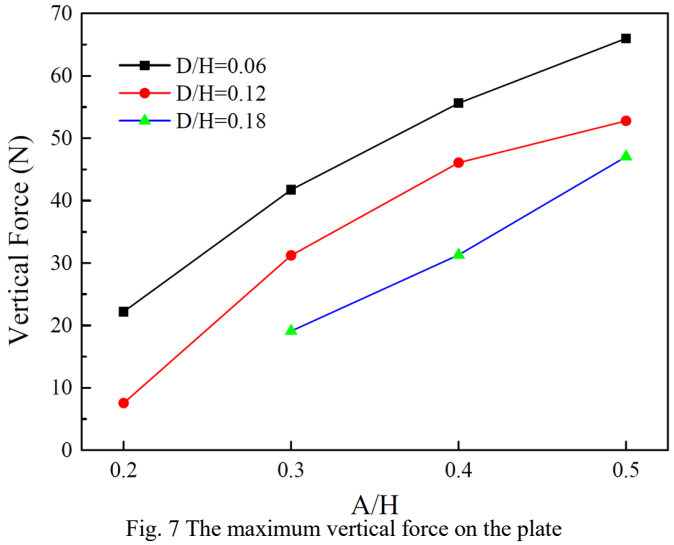

Fig. 7 The maximum vertical force on the plate

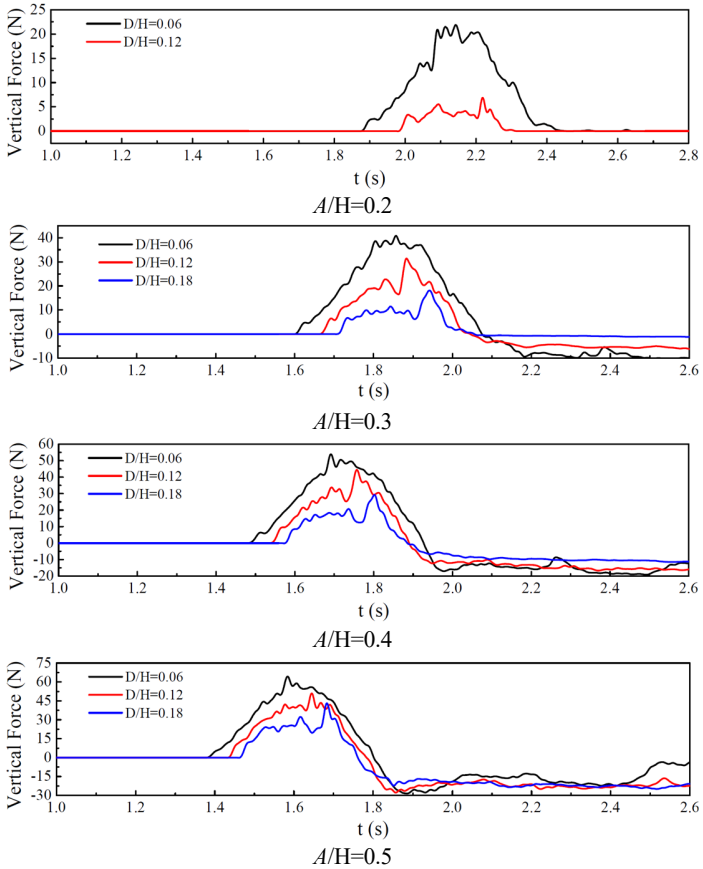

Fig. 8 History of the vertical force on the plate

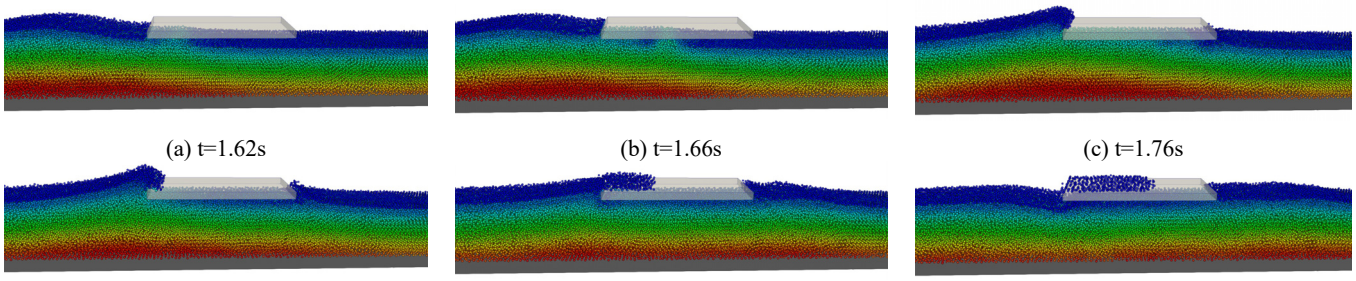

(a) t=1.62s (b) t=1.66s (c) t=1.76s

(d) t=1.80s (e) t=1.92s (f) t=2.04s

Fig. 9 Snapshots of wave-plate interaction (rigid plate)

The influence of the structure flexibility on slamming

In this subsection, the interaction between the solitary wave and a rigid plate is simulated with *A*/H=0.3, *D*/H=0.1. The result is compared with the flexible case in order to investigate the contribution of the structural flexibility to the wave-induced force and energy dissipation. Some particular snapshots in the selected simulation are given in Fig. 9. The history of wave-induced force on plate is shown in Fig. 10. It can be seen that at around t=1.62s the wave contacts the leading edge of plate and impacts the plate. When the wave crest hits the leading edge of plate at around 1.76s, the vertical force reaches maximum. At 1.82s, evident spray and wave breaking can be observed behind the plate, which dissipate energy from the system, resulting to a drastic drop in the curve of vertical force.

Compared with the flexible plate's counterpart, evident differences can be observed in the vertical force. For the rigid plate, it takes only 0.16 second to reach the maximum vertical force, then the vertical force descends drastically with evident oscillation. However, in the flexible plate, the maximum vertical force lags slightly and lasts for one second with sight oscillation, besides, the maximum vertical force is lower than the rigid case. Then there is no obvious oscillation during the descending of the vertical force. The reason for these differences probably is that the upward displacement due to the impact provides a cushioning for wave to spend more time on suffusing the bottom of flexible plate, so it leads to the difference in loading time of vertical force. Moreover, it also results to a lower peak value for flexible plate. In addition, the comparison of horizontal force between rigid and flexible plate shows a fair agreement, while there are some evident oscillations in the flexible case.

The velocity distribution of the fluid field is depicted in Fig.11. When the solitary wave has no contact with the plate, the velocity vector of the water particle is acclivitous, and when the wave contacts the plate, the velocity vector of water particle near the leading edge of the plate is almost perpendicular to the horizontal plate, in both two cases. However, the fluid under the plate presents evident difference. In the rigid plate, the velocity vector is basically parallel to the plate during the whole impact. While in the flexible plate, the velocity vector is inclined to the plate during the slamming stage, then the velocity vector is downward to the plate during the post stage, shown in Fig.11 (b ~ c). In addition, during the post stage, evident spray can be observed behind the rigid plate, which does not exist in the flexible plate. Besides, the velocity transmitting from the aft end of rigid plate is obviously smaller than that of flexible plate. The discrepancy of energy is the reason for the above difference. For the flexible case, energy transfer is mainly taken into account: During the slamming stage, the plate absorbs some of the wave energy due to the upward deformation, then it returns most energy to the fluid under the plate. While in the rigid case, energy dissipate is primary important: An evident spray behind the aft end of the plate during the post stage is an evident proof to the energy dissipate, as well as the smaller velocity transmitting from the aft end of plate. Consider the above reasons, during the impact, the energy is shown to dissipate, particularly in rigid plate. It illustrates that wave attenuation is more significant in the rigid case than the flexible case. It is similar to the results of the experiment of Nelli et al (2017).

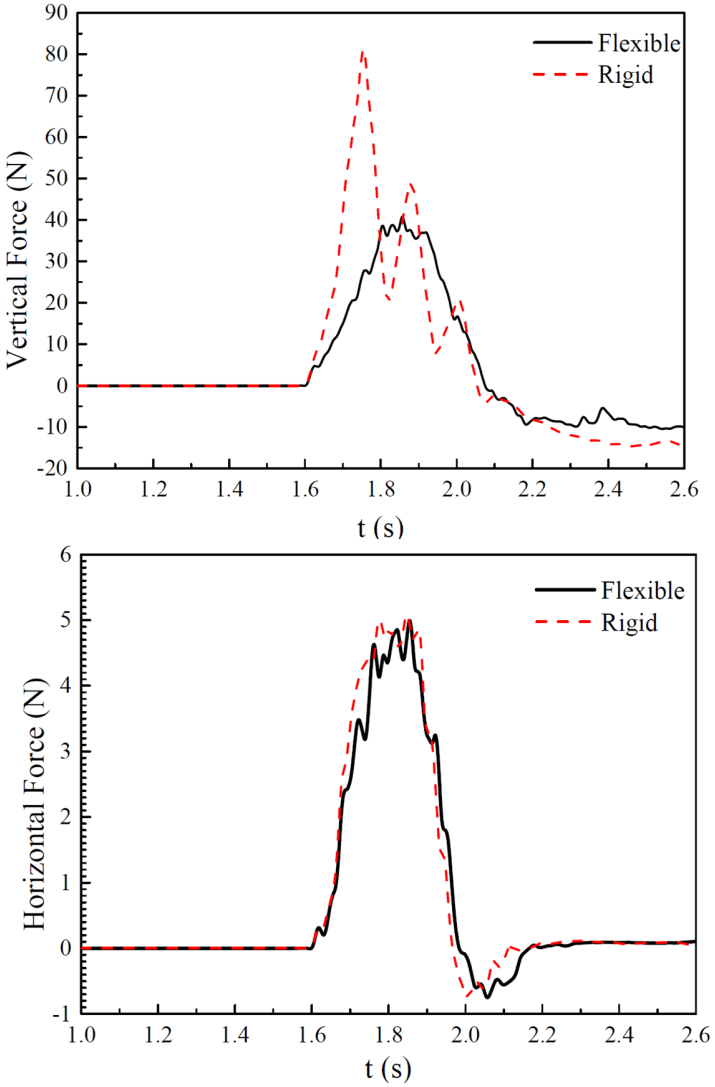

Fig. 10 History of wave-induced forces on plate

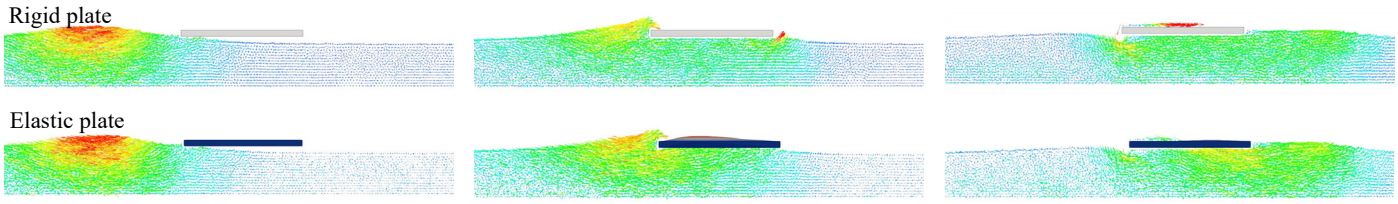

(a) t=1.60s (b) t=1.76s (c) t=2.04s

Fig. 11 The velocity distribution of the fluid field (Top panels are rigid plate; Bottom panels are flexible plate)

CONCLUSIONS

In present paper, the interaction between the solitary wave and the horizontal flexible plate is numerically investigated based on aforementioned MPS-FEM coupled method. Based on the results of simulations, the following conclusions can be summarized as follows:

The wave amplitude (A/H=0.2, 0.3, 0.4 and 0.5) and plate elevation (D/H=0.06, 0.12 and 0.18) are first taken into account to study their effects on the interaction. The results indicate that the maximum vertical force is in proportion to the wave amplitude, while the maximum vertical force decreases with the ascending of the elevation. In addition, the loading duration increases with the ascending of the amplitude, as well the descending of the elevation. Evident oscillation during the rise of force can be observed in a greater elevation.

Subsequently, the wave-induced force is primarily focused in this research to study the effects of flexibility on wave-plate interaction. The interaction between the solitary wave and a flexible plate is simulated under the condition of A/H=0.3 and D/H=0.1, compared with the rigid plate. The discrepancies in vertical force help us clearly observe the contribution of the structural flexibility. In the flexible case, the upward displacement due to the impact provides a cushioning for wave to spend more time on suffusing the bottom of the plate, so it leads to the difference in loading time of vertical force. Moreover, it also results to a lower peak value for flexible plate. However, the comparison of horizontal force between rigid and flexible plate shows a fair agreement, which indicates that the interaction between wave and plate mainly reflects in vertical slumming.

Simultaneously, the analysis of flow field for rigid and flexible plate shows the contribution of the structural flexibility to the energy. For the flexible case, energy transfer is mainly taken into account, while in the rigid case, energy dissipate is primary important. It illustrates that, the energy is shown to dissipate during the impact, particularly in rigid plate. So, wave attenuation is more significant in the rigid case than the flexible case. The conclusion is similar to the results of the experiment of Nelli et al (2017).

ACKNOWLEDGEMENTS

This work is supported by the National Natural Science Foundation of China (51490675, 11432009, 51579145), Chang Jiang Scholars Program (T2014099), Shanghai Excellent Academic Leaders Program (17XD1402300), Program for Professor of Special Appointment (Eastern Scholar) at Shanghai Institutions of Higher Learning (2013022), Innovative Special Project of Numerical Tank of Ministry of Industry and Information Technology of China (2016-23/09) and Lloyd's Register Foundation for doctoral student, to which the authors are most grateful.

REFERENCES

Antoci, C, Gallati, M, and Sibilla, S (2007). "Numerical Simulation of Fluid–structure Interaction by SPH," *Computers and Structures*, 85(11), 879-890.

Attaway, SW, Heinstein, MW, and Swegle, JW (1994). "Coupling of Smooth Particle Hydrodynamics with the Finite Element Method, " *Nuclear engineering and design*, 150(2-3), 199-205.

Cox, DT, and Ortega, JA (2002). "Laboratory observations of green water overtopping a fixed deck," *Ocean Engineering*, 29(14): 1827-1840.

Cuomo, G, Tirindelli, M, and Allsop, W (2007). "Wave-in-deck loads on exposed jetties," *Coastal Engineering*, 54(9), 657-679.

Fourey, G, Oger, G, Touzé, DL, and Alessandrini, B (2010). "Violent Fluid-Structure Interaction Simulations using a Coupled SPH/FEM method," *Iop Conference Series Materials Science & Engineering*, 10, 012041.

Goring, DG (1978). "Tsunamis-the Propagation of Long Waves onto a Shelf," PhD thesis, California Institute of Technology, Pasadena, California, USA.

Gotoh, H, and Khayyer, A (2016). "Current achievements and future perspectives for projection-based particle methods with applications in ocean engineering," *Journal of Ocean Engineering and Marine Energy*, 2(3), 251-278.

Hwang, SC, Khayyer, A, Gotoh, H, and Park, JC (2014). "Development of a Fully Lagrangian MPS-based Coupled Method for Simulation of Fluid-structure Interaction Problems," *Journal of Fluids & Structures*, 50(2), 497-511.

Hwang, SC, Park, JC, Gotoh, H, Khayyer, A, and Kang, KJ (2016). "Numerical Simulations of Sloshing Flows with Elastic Baffles by using a Particle-based Fluid-structure Interaction Analysis Method," *Ocean Engineering*, 118, 227-241.

Hsiao, KM, Lin, JY, and Lin WY (1999). "A Consistent Corotational Finite Element Formulation for Geometrically Nonlinear Dynamic Analysis of 3-D Beams," *Comput. Methods Appl. Mech. Engrg*, 169, 1-18.

Irajpanah K (1983). "Wave uplift force on horizontal platform," PhD thesis, University of Southern California, Los Angeles, USA.

Korteweg DJ, and De Vries, G (1895). "On the change of form of long waves advancing in a rectangular canal, and on a new type of long stationary waves," *Philosophical Magazine*, 39(240), 422-443.

Koshizuka, S, and Oka, Y (1996). "Moving-particle Semi-implicit Method for Fragmentation of Incompressible Fluid," *Nuclear science and engineering*, 123(3), 421-434.

Lee, BH, Park, JC, Kim, MH, and Hwang, SC (2011). "Step-by-step improvement of mps method in simulating violent free-surface motions and impact-loads," *Computer Methods in Applied Mechanics & Engineering*, 200(9-12), 1113-1125.

Lee, CJK, Noguchi, H, and Koshizuka, S (2007). "Fluid–shell Structure Interaction Analysis by Coupled Particle and Finite Element Method," *Computers and structures*, 85(11), 688-697.

Liao, K, and Hu, C (2013). "A Coupled FDM-FEM Method for Free Surface Flow Interaction with Thin Elastic Plate," *Journal of marine science and technology*, 18(1), 1-11.

Lucy, LB (1977). "A Numerical Approach to the Testing of the Fission Hypothesis," *The astronomical journal*, 82, 1013-1024.

Long, T, Hu, D, Yang, G, and Wan, D (2016). "A Particle-element Contact Algorithm Incorporated into the Coupling Methods of FEM-ISPH and FEM-WCSPH for FSI Problems," *Ocean Engineering*, 123, 154-163.

Liu, M (2016). "Experimental Study of Wave Slamming on Flat Plate Construction with Elastic Support," PhD thesis, Dalian University of Technology, China (In Chinese).

Liu, X, and Sakai, S (2002). "Time Domain Analysis on the Dynamic Response of a Flexible Floating Structure to Waves," *Journal of Engineering Mechanics*, 128(1), 48-56.

Liu, K, Liu, B, Villavicencio, R, Wang, ZL, and Soares, CG (2018). "Assessment of material strain rate effects on square steel plates under lateral dynamic impact loads," *Ships and Offshore Structures*, 13(2), 217-225.

Mitsume, N, Yoshimura, S, Murotani, K, and Yamada, T (2014). "Improved MPS-FE Fluid-structure Interaction Coupled Method with MPS Polygon Wall Boundary Model," *Computer Modeling in Engineering & Sciences*, 101(4), 229-247.

Nelli, F, Bennetts, LG, Skene, DM, Monty, JP, Lee, JH, Meylan, MH, and Toffoli, A (2017). "Reflection and transmission of regular water waves by a thin floating plate," *Wave Motion*, 70, 209-221.

Newmark, NM (1959). "A Method of Computation for Structural Dynamics," *Journal of the engineering mechanics division*, 85(3), 67-94.

Rao, CP, Zhang, YL, and Wan, DC (2017). "FSI analysis of solitary wave interacting with horizontal flexible plate by MPS-FEM Method," *The 27th International Ocean and Polar Engineering Conference*, June 25-30, San Francisco, California, USA, 263-272.

Seiffert, B, Hayatdavoodi, M, and Ertekin, RC (2014). "Experiments and Computations of Solitary-wave Forces on a Coastal-bridge Deck. Part I: Flat Plate," *Coastal Engineering*, 88, 194-209.

Tanaka, M, and Masunaga, T (2010). "Stabilization and smoothing of pressure in mps method by quasi-compressibility," *Journal of Computational Physics*, 229(11), 4279-4290.

Tang, ZY, and Wan, DC (2015). "Numerical Simulation of Impinging Jet Flows by Modified MPS Method," *Engineering Computations*, 32 (4), 1153-1171.

Tang, ZY, Zhang, YL, and Wan, DC (2016). "Multi-resolution MPS Method for Free Surface Flows," *International Journal of Computational Methods*, 13 (4), 1641018.

Yang, Q, Jones, V, and McCue, L (2012). "Free-surface Flow Interactions with Deformable Structures using an SPH-FEM Model," *Ocean Engineering*, 55, 136-147.

Zhang, YL, Chen, X, and Wan, DC (2016a). "An MPS-FEM Coupled Method for the Comparative Study of Liquid Sloshing Flows Interacting with Rigid and Elastic Baffles," *Applied Mathematics and Mechanics*, 37(12), 1359-1377 (In Chinese).

Zhang, YL, Tang, ZY, and Wan, DC (2016b). "MPS-FEM Coupled Method for Interaction between Sloshing Flow and Elastic Structure in Rolling Tanks," *Proceedings of the 7th International Conference on Computational Methods*, August 1-4, Berkeley, USA, No. 1493-6106-1-PB.

Zhang, YL, and Wan, DC (2017). "Numerical Study of Interactions between Waves and Free Rolling Body by IMPS Method," *Computers and Fluids*, 155: 124-133.

Zhang, YL, and Wan, DC (2018). "MPS-FEM coupled method for sloshing flows in an elastic tank." *Ocean Engineering*, doi.org/10.1016/j.oceaneng.2017.12.008.

Zhang, YX, and Wan, DC (2012). "Apply MPS Method to Simulate Liquid Sloshing in LNG Tank," *Proceedings of 22nd International Offshore and Polar Engineering Conference*, June 17-23, Rhodes, Greece, 381-391.

Zhang, YX, Wan, DC, and Hino, T (2014). "Comparative Study of MPS Method and Level-set Method for Sloshing Flows," *Journal of hydrodynamics*, 26(4), 577-585.